On-line Partial Discharge Localization of 10-kV Covered Conductor Lines

On-line Partial Discharge Localization of 10-kV Covered Conductor Lines

Yuan Yan, Yinsong Zhao, Weisheng He, Igor S. Stievano , *Senior Member, IEEE*, and Hongjie Li

***Abstract*—This paper proposes an innovative partial discharge (PD) location technique for overhead electrical power distribution networks. It is aimed at improving the condition-based maintenance of the network. PD localization is carried out via an improved double-sided traveling-wave method. The method is driven by a hybrid detection technique, which integrates a pulse-based synchronization mechanism and a global positioning system (GPS). The proposed solution offers a number of benefits. It has the nice inherent feature of being immune to varying physical parameters of the transmission line, and it has been proven be offer improved accuracy with respect of the conventional GPS-based location methods. Also, an in-house designed portable and non-invasive test setup is presented and thoroughly discussed, thus demonstrating the feasibility of the proposed method. Moreover, an enhanced algorithm is embedded into the PD location system to improve robustness to high-level noise. Finally, the proposed tool relies on a well-established automatic procedure which requires neither parameter tuning nor any expert intervention. The features and strengths of the method are validated on a real case consisting of a 2125-m long 10-kV overhead covered conductor line.**

***Index Terms*—Partial discharge localization, travelling wave method, time synchronization, pulse time-of-arrival and polarity analysis, least-squares approach.**

I. Introduction

A. Background

Insulation failures in electrical apparatus can cause power outages, disrupting customers' daily activities and harming the economy. The solution to this problem is to conduct condition-based maintenance of the equipment which is a strategy to optimize maintenance and operation actions from the asset/grid management side by evaluating the operating condition indicators of electrical equipment [1]. Partial discharge (PD), a phenomenon able to reveal or cause incipient failure of electrical apparatus, plays a fundamental role in maintenance [2]. Regular PD diagnosis can predict the upcoming insulation failures, enabling electric utilities to repair or remove the defective apparatus in a timely manner [3].

10-kV overhead covered conductor (CC) lines are one of the major electrical objects in distribution networks. They are frequently affected by PDs caused by diverse weather conditions, falling trees, and many other environmental stresses [4]. Traditionally, technicians patrol along CC lines to identify PDs by the vision- and ultrasonic-based method [5,6]. However, this method is not only insensitive to the PDs that occur inside the electrical equipment, but also laborious and time-consuming to use for CC lines in large distribution networks. To overcome these limitations, electromagnetic-based measurement techniques, which can remotely detect PD, were recently developed [4,7-10]. In this techniques, PD localization is promising because it provides target maintenance indicators that enable highly efficient condition-based maintenance of CC lines. However, synchronization problems, varying and possibly unknown precise values of the physical parameters of the transmission lines, and field interferences make PD localization challenging, thus requiring improvements of existing techniques.

B. Related work

Traveling-wave (TW) methods, which are the most popular PD location method for power lines, fall into two categories: time domain reflection (TDR) and arrival time analysis (ATA). TDR locates PDs by calculating the difference of TOAs between a pulse and its reflection arriving at the same end [11]. ATA locates PDs by calculating difference of TOAs of the pulses arriving at double or multiple ends [12]. The complex structures of 10-kV CC lines produce many impedance discontinuities, leading to undefinable reflections. This causes TDR to fail to locate PDs in CC lines. In contrast, the double-sided TW method based on ATA is immune to the reflections, so its ability to locate PDs in CC lines has been validated [13]. However, the difficulty in synchronization of the PD detectors has posed a challenge for the double-sided TW method.

Global position system (GPS) is the most widely used synchronization technique, but its synchronization precision fluctuates and it is affected by environmental factors. In previous papers [14,15], an alternative synchronization technique was explored. This technique uses injected pulses to synchronize double-sided PD detectors in CC lines, which was inspired by the pulse synchronization technique presented in [16]. However, the in-field reliability of this pulse synchronization technique is low because it often fails in a noisy environment where PD pulses or interferences have the

This work was supported in part by China Scholarship Council, and also by Taizhou Power Supply Branch of State Grid Jiangsu Electric Power Co., LTD. (corresponding author: hjli@mail.xjtu.edu.cn)

Yuan Yan is with State Key Laboratory of Insulation and Power Equipment, School of the Electrical Engineering, Xi'an Jiaotong University, Xi'an, 710049, China, and also with Department of Electronics and Telecommunications, Politecnico di Torino, Turin, 10129, Italy.

Yinsong Zhao and Hongjie Li are with State Key Laboratory of Insulation and Power Equipment, School of the Electrical Engineering, Xi'an Jiaotong University, Xi'an, 710049, China.

Weisheng He is with School of Electronics and Information, Chongqing University of Posts and Telecommunications, Chongqing, 400065, China.

Igor S. Stievano is with Department of Electronics and Telecommunications, Politecnico di Torino, Turin, 10129, Italy.

same amplitude as the injected pulses.

The physical parameters of CC lines (e.g., structure and height) and their surrounding environment are complex and diverse. This means that signals propagate at a variety of velocities in CC lines, which may generate non-negligible PD location errors [4,17]. Reference [17] describes a multi-end correlation-based method that was adapted to eliminate the effect of varying velocities on PD localization in CC lines. However, the accuracy of this method could be significantly reduced when the waveform of PD pulses in CC lines is distorted by high-frequency attenuation or signal overlapping.

In on-line PD measurement, different kinds of electromagnetic interferences can reduce the accuracy of PD localization and even cause inconsistent PD locations. These interferences mainly consist of continuous noise interferences (CNIs) and impulse noise interferences (INIs) [9,10]. CNIs can be successfully suppressed by a time-frequency de-noising technique, such as discrete wavelet transforms (DWT) [18,19]. By contrast, removing INIs from noisy signals is still a difficult task because their features are quite similar to those of real PDs.

C. Contribution and paper organization

The limitations of the above-mentioned PD location methods for CC lines motivated our current study, which offers the following main contributions and improvements.

1) A hybrid time-synchronization technique, achieved by a GPS-triggered pulse-based synchronization mechanism (GPSM), is proposed to improve the conventional double-sided TW method. It combines the advantages of GPS's stability and PSM's accuracy, thus enabling reliable and accurate PD localization.
2) An on-line PD location system for CC lines, consisting of two portable and non-invasive testing units and a cloud server, is developed to demonstrate the real-life feasibility of the proposed technique.
3) A simple yet effective PD location algorithm is devised. It suppresses CNIs via DWT, removes INIs via a pulse TOA-polarity analysis, and estimates an accurate PD location via least-squares approach. This enables accurate and effective PD location in noisy environments.

The rest of this paper is structured as follows. In Section II, the proposed PD location method is presented. In Section III, implementation of the on-line PD location system is described in details. In Section IV, the development of the PD location algorithm is described. In Section V, laboratory and field validation of the proposed method, system, and algorithm are thoroughly discussed. Conclusions and final remark are drawn in Section VI.

II. Method for PD Localization of CC Lines

A. Classical PD localization via the double-sided TW method

The fundamental principle of the method is shown in Fig. 1. As a PD defect occurs on a CC line or its tips, the TW pulses produced by the defect propagate to both sides along the CC line. Thus, the location of the PD defect can be determined by calculating difference of TOAs of the TW pulses between the two PD detectors mounted on the two sides of the CC line. The distance l_{PD} from a PD to Side A can be calculated as:

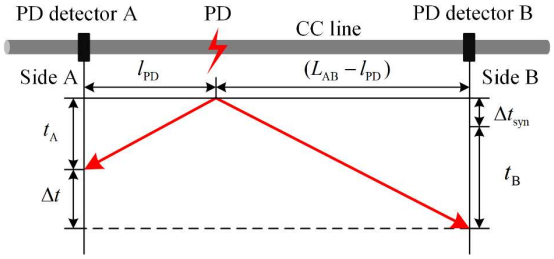

Fig. 1. Schematic of the classical double-sided PD localization on a CC line section based on ATA.

$$l_{PD}=\frac{L_{AB}+[t_A-(t_B+\Delta t_{syn})]\cdot v}{2} \quad (1)$$

where t_A and t_B are the TOAs of PD pulses at Side A and B, L_{AB} is the length of the CC line, Δt_{syn} is the synchronization error between the two PD detectors, and v is the velocity of the PD signal propagating in the CC line. It follows that the errors or inconsistencies in determining PD source locations are due to synchronization errors, propagation velocity errors, and TOA errors. These errors must be minimized for accurate PD localization.

B. Improved double-sided PD localization driven by GPSM

Synchronization errors and propagation velocity errors are the most critical aspects of the above double-sided TW method. To minimize them, GPSM, a hybrid time-synchronization technique is devised. It integrates a pulse-based synchronization mechanism (PSM) and a GPS. GPSM enables accurate (due to the PSM) and reliable (due to the GPS) synchronization of the double-sided PD detectors and calculation of the signal propagation velocity. A seven-step overview of the working procedure of GPSM is detailed below (see Fig. 2).

1) Two PD detectors and two pulse injectors are mounted on each side of a target section of CC line.
2) PD detectors on Side A and B both start to acquire data when they are activated by their respective GPS triggers. PSM is only triggered within a short pre-set time-window.
3) On side A, at the beginning of the time window, a high-amplitude pulse $V_{SYN,A1}$ is generated and inductively injected into the CC line at time t_1 by the pulse injector.
4) $V_{SYN,A1}$ propagates from side A along the CC line and arrives, in an altered form, at side B after propagation time T. This altered pulse is denoted $V_{SYN,B1}$.
5) The PD detector on side B captures $V_{SYN,B1}$ at time t_2. Another high amplitude pulse, $V_{SYN,B2}$, is then generated and inductively injected into the CC line at t_3. The latter parameter t_3 is controllable and it is set to be significantly larger than $(t_1+\Delta t_{syn}+T)$ to ensure that $V_{SYN,B2}$ occurs later than $V_{SYN,B1}$, i.e., $t_2<t_3$. Since Δt_{syn} fluctuates within a few microseconds at most, and T can be approximately estimated with the length of the CC line, it is easy to ensure $t_2<t_3$ by setting a large enough interval (e.g., T+20

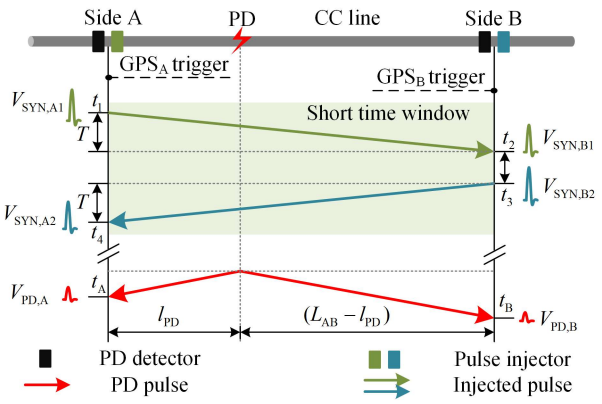

Fig. 2. Illustration of the improved PD location method for CC lines based on the proposed GPSM.

μs) between t_3 and t_1.

6) $V_{SYN,B2}$ propagates from side B along the CC line and arrives, in an altered form, at Side A after time T, at t_4. This altered pulse is denoted $V_{SYN,A2}$. At this time, PSM is completed and the time window soon ends. In the PSM, synchronization of the double-sided PD detectors and estimation of the propagation velocity can be achieved, as described as follows.

First, by calculating the TOAs of the injected pulses, the propagation time T from Side A to Side B can be calculated as:

$$T=\frac{(t_4-t_1)-(t_3-t_2)}{2} \tag{2}$$

Second, it is assumed that t_1 represents the absolute time reference for the signal acquired on Side A. Thus, as the absolute TOA difference between $V_{SYN,A1}$ and $V_{SYN,B1}$ equals propagation time T, the absolute time reference for the signal acquired on Side B is (t_2-T). Therefore, Δt_{syn}. in Equation (1) can be calculated as:

$$\Delta t_{syn}=t_1-t_2+T \tag{3}$$

Third, using the calculated propagation time T and the length L_{AB} of the measured CC line section, the signal propagation velocity (v) of the target CC line section can be calculated as:

$$v=\frac{L_{AB}}{T} \tag{4}$$

7) The double-sided PD detectors continue to acquire PD data for more than one power-frequency cycle. Two pulses, $V_{PD,A}$ and $V_{PD,B}$, which originate from the same PD activity, are used to represent the test results for Side A and Side B, respectively. In addition, t_A and t_B are the arrival times of $V_{PD,A}$ and $V_{PD,B}$, respectively. Therefore, incorporating Equation (1), (2), (3) and (4), the PD location (l_{PD}) can be calculated as:

$$l_{PD}=\frac{L_{AB}\cdot[(t_A-t_1)-(t_B-t_2)]}{(t_4-t_1)-(t_3-t_2)} \tag{5}$$

In contrast to Equation (1), Equation (5) eliminates synchronization errors and propagation velocity errors, thus enabling more accurate PD localization.

III. Implementation of an On-line PD Location System for CC Lines

A. Overview of the system

This section describes an in-house developed on-line PD location system for CC lines based on the above-presented method. The main components of the system and one of its typical application scenario are illustrated in Fig. 3. The system includes a 5G-based cloud server and two portable and non-invasive testing units mounted on each side of a target CC line section. The main hardware components of each testing unit are three PD detectors, a pulse injector, and an analyzer. All parts are connected via fiber-optic cables, which ensures that a user is adequately isolated from high voltages. The details of the system are described in the following subsections.

B. PD detector

High frequency current transformer (HFCT) is used as the sensor in the PD detectors because of its high sensitivity, wide frequency band, and non-invasive placement. At an on-line testing situation, all measuring instruments must be kept at a sufficient insulation distance from the high-voltage CC lines [20]. Thus, an improved PD detector is developed. It consists of a modified HFCT, an instrumentation amplifier, a battery, and an electrical-optical converter, as shown in Fig. 4. The modified HFCT consists of an incomplete circular ferrite core with a 90-degree gap and 15 turns coils. The gap in the core can avoid the magnetic saturation caused by the power frequency current in the CC line. The frequency passband of the instrumentation amplifier is from 0.1 MHz to 82 MHz. The electrical-optical converter (HFBR1412, BROADCOM), which has a good linearity and a wide frequency range from DC to 125MHz, is used. The detection sensitivity of the PD detector is approximately 5.6 mV/mA over a dynamic range of −204 to 206 mA, and its −6 dB frequency bandwidth is approximately 0.2 MHz-50 MHz, as shown in Fig. 5. The wide frequency pass-band allows the PD detector to accurately detect the fast-rising edge of PD pulses and collect as much energy of PD pulses as possible. Nevertheless, it is important to point out that the wideband property of the PD detector leads to an increased susceptibility of the PD detection to the field noise. Therefore, noise reduction is an essential task and it will be discussed in details in Section IV.

C. Pulse injector

Figure 6 depicts the internal structure of a pulse injector, showing its pulse-injection coils, an optical-electrical converter (HFBR2416, BROADCOM), a battery, and a simplified high-amplitude pulse generator. The mutual inductance between the pulse-injection coils and the CC line is used to couple the high-amplitude pulses produced by the pulse generator into the CC line. An amorphous magnetic core with a high magnetic permeability of 5000 is used in the pulse-injection coils to increase the mutual inductance. The DE475-102N21A (IXYS) model of the RF power metal-oxide-semiconductor field-effect transistor, G, is selected; it has fast switching speed of 200V/ns.

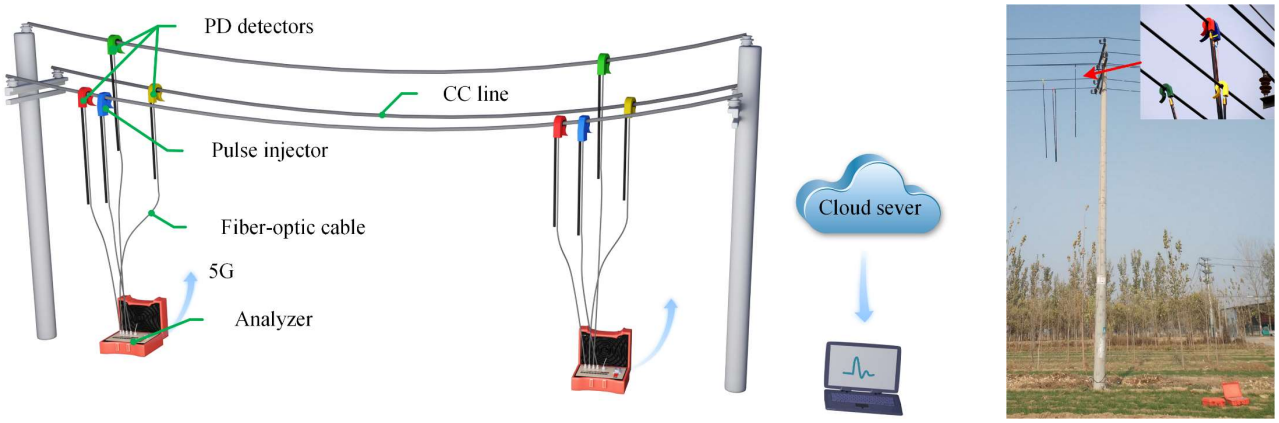

(a) (b)

Fig. 3. Simplified representation of a typical application scenario (a) and field installation (b) of the developed on-line PD location system.

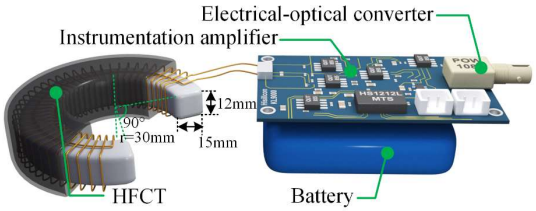

Fig. 4. Internal structure of a PD detector.

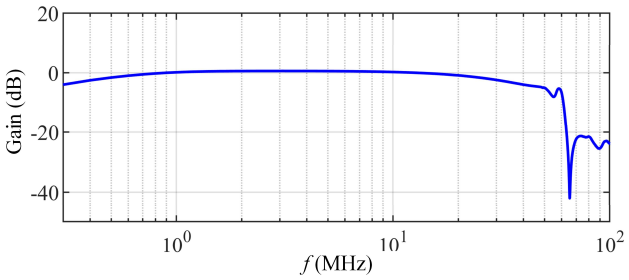

Fig. 5. Transmission frequency-response curve of the designed PD detector.

The equivalent circuit of a simplified pulse generator is depicted in Fig. 7. First, the transistor G is opened and the 1,000-V DC supply charges the capacitor C in the presence of the current-limiting resistance R. Next, G is closed. As a result, a high-amplitude pulse is produced on the coils and partly coupled into the CC line via the mutual inductance M_0. Figure 8 depicts the voltage waveform of a pulse injected into a 3-m CC line. It can be seen that a high-amplitude pulse, with a voltage peak of 177.3 V, a rising time of 12 ns, and a 50%-peak pulse-width of 402 ns, was successfully injected into the CC line.

D. Analyzer

The analyzer consists of four parts: a measurement module, a central processing unit module, a 5G communication module (5G RG200U-CN, QUECTEL), and a commercial GPS module (UM220-III, UNICORECOMM). The measurement module has three optical-electrical converters for PD detection, an electrical-optical converter for pulse injection, and a three-

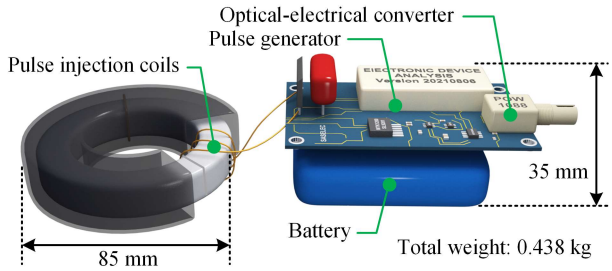

Fig. 6. Internal structure of a pulse injector.

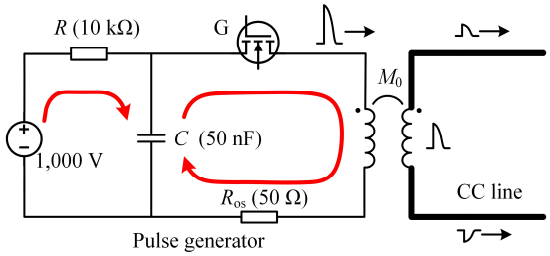

Fig.7. Equivalent circuit of the pulse generator and the pulse injection coils.

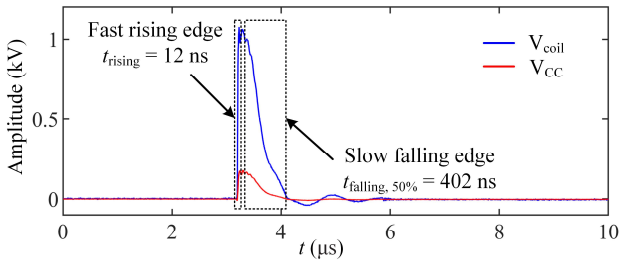

Fig. 8. Voltage waveforms of the injected pulses on the pulse-injection coils (blue line) and the CC line (red line).

channel analog-to-digital converter (ADC) with a sampling rate of 125 MS/s. Time base errors between the ADCs in the double-sided analyzers can deviate their sampling rate slightly from 125MS/s, which can lead to non-negligible PD location errors. Thus, the conventional voltage-controlled crystal oscillator in the commercial ADC is replaced by the constant temperature crystal oscillator (AOCJY7TQ, ABRACON) in the developed

analyzers for PD location application. AOCJY7TQ has less than 0.05 ppm frequency error in the temperature range from -40℃ to 70℃. In other words, time base errors between the two improved ADCs can be less than 5ns while the whole sampling time is up to 120ms.

IV. Development of an Enhanced PD Location Algorithm for CC Lines

When applied to real CC lines, the developed PD location system will inevitably be affected by noise interferences. Two signals ($\mathbf{x}_A$ and $\mathbf{x}_B$) from a real 5,232-m CC line with a PD defect (on a grimy insulator 4,691 m along the line) are shown in Fig. 9. The signals contain not only PD pulses but also a high level of noise. In the time domain, this noise is typically composed of either CNIs or INIs. CNIs include white noise and discrete spectrum noise, and INIs include repeated pulse noise and random pulse noise [9, 10]. From the example waveform of Fig. 9, it is important to point out that the starting part of the PD pulses is cluttered by the CNI, which unavoidably leads to a imprecise estimation of the TOA parameter of the PD pulse. On the other hand, also the INI possibly lead to errors in determining the PD location, mainly due to its inherent feature of sharing some waveform similarities with the functional PD pulses. Thus, to suppress the influence of such interferences, a specific PD location algorithm is devised. The overall framework of the algorithm is shown in Fig. 10, and its detailed explanation is described in the following subsections.

A. Suppression of CNIs and extraction of pulse TOAs, peaks, and polarities

Since the PD signals are non-stationary and transient, their energy spreads over the whole band and merges with the noise if it is extracted using continuous and periodic base (sine and cosine) functions [18]. DWT, which can achieve both high frequency resolution and accurate time resolution, has proven to be one of the most effective methods in rejecting different kinds of interferences from the noisy PD signal [18, 19]. Therefore, in this work, DWT are used to de-noise the PD signal. Here, DWT tool supported by MATLAB is used to suppress CNIs and its parameter selection is discussed as follows.

Daubechies wavelets (db8), which have the same shape as PD pulses [19], are used as the mother wavelets to decompose the acquired signals. In principle, the number of decomposition levels in DWT should be determined according to the frequency spectrum of the PD signal. However, since the frequency spectrum is unknown in field measurement (e.g., due to the unavoidable effects of location, size, and material of the PD defect), the number of the decomposition levels is determined based on the low cut-off frequency of the PD detector. On the one hand, the number of decomposition levels must large enough to ensure that the measured PD signal can be fully decomposed, which is equivalent to choosing the top-level frequency bandwidth in the DWT to be lower than the low cut-off frequency of the PD detector. On the other hand, a possibly large value of the decomposition levels yields unnecessary additional computational overhead. For the example at hand, the above number turns out to be 9. In this case, the frequency bandwidth of decomposed signals is equal to 125

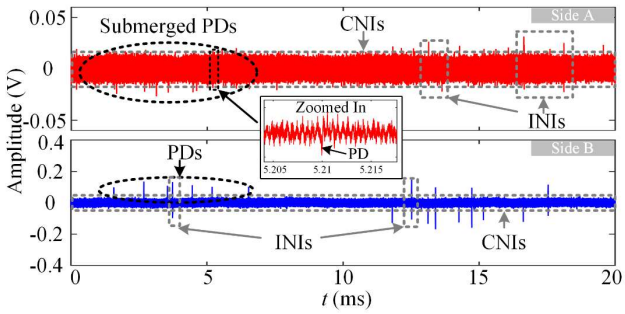

Fig. 9. Waveforms of two 20-ms noisy signals acquired by two PD detectors mounted on the same phase of a real 5232-m CC line with a PD defect (on a grimy insulator 4691-m along the line).

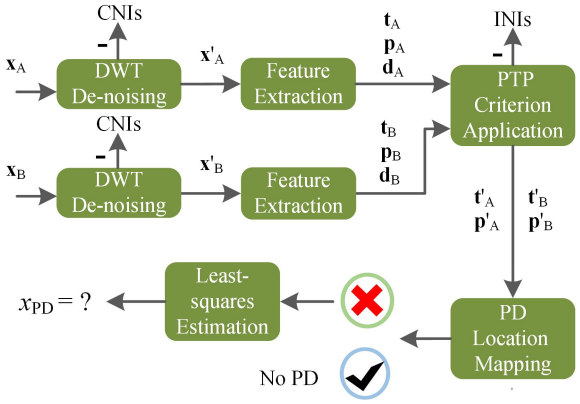

Fig. 10. Block diagram of the entire PD location algorithm.

MHz/2/2^9=0.122 MHz, which is lower than the lower cut-off frequency of the PD detector (i.e., 0.2 MHz), thus allowing a sufficient frequency resolution to process the PD signals collected by the developed PD detector. In addition, an automated thresholding technique based on the soft-thresholding function is employed to suppress the continuous noise in each level via a formula in [19]. Finally, modified wavelet coefficients are then used to apply an inverse DWT and achieve data recovery.

The key features of pulses in the signals de-noised by DWT, including TOAs, peaks, and polarities, were then extracted. First, a threshold based on 3σ-rule [21] is defined to seek pulses. The threshold value is equal to three times the standard deviation of the de-noised signal. Second, the TOAs of the identified pulses are calculated using the energy criterion (EC), as this method was found to give the best accuracy and robustness for noisy signals [22]. EC is completed in a short time window (N_{win} = 500) and the target pulse is shifted to the middle of the time window. The PD energy is defined as:

$$E = \sum_{k=0}^{N_{\text{win}}} u_{\text{PD},k}^2 \tag{6}$$

where $u_{\text{PD},k}$ denotes the sampling value of $\mathbf{x}'_A$ or $\mathbf{x}'_B$ in the time window. Using the E, the EC is built as:

$$EC(i) = \sum_{k=0}^{i} u_{\text{PD},k}^2 - i \cdot \frac{E}{N_{\text{win}}} \tag{7}$$

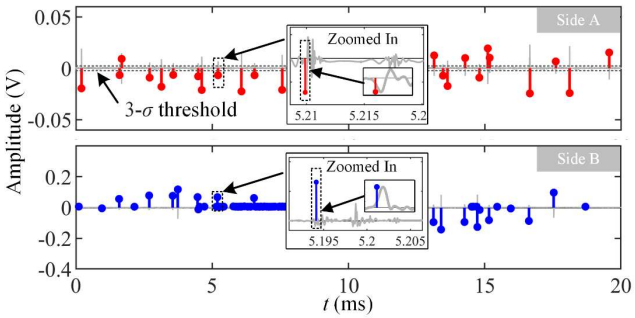

Fig. 11. TOAs, peaks, and polarities extracted from the pulses in the noisy signals in Fig. 9. The zoomed in inset displays the extracted details, where reflections are removed. The gray lines denote the signals de-noised by the DWT, and the red stems and the blue stems denote the signs of the features of the pulses.

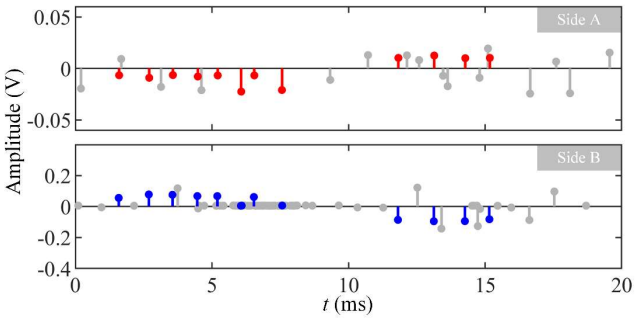

Fig. 12. Signs of the pulses remaining after applying a PTP criterion to the feature extraction results in Fig. 11. The red and blue stems denote the remaining pulses, and the gray stems denote all pulses before applying the PTP criterion.

The minimum value of $EC(i)$ represents the EC onset position and is defined as the TOA of the pulse. Then, peaks and polarities of the pulses are calculated. A peak is defined as the first point over the threshold and after the TOA, where the trend of the first-order difference changes from positive to negative or from negative to positive. If the first-order difference changes from positive to negative, the polarity of the pulse is defined as positive, i.e. 1; if it changes from negative to positive, the polarity is defined as negative, i.e. −1.

TOAs, peaks, and polarities of PDs, INIs, and their reflections are all obtained. These reflections are always caused by impedance discontinuities at branch joints, which is inevitable in real CC lines. However, these reflections are unacceptable because they could lead to incorrect PD locations. Since the time interval between two adjacent PD pulses (e.g., several hundreds of μs) is significantly larger than that between a PD pulse and its reflections (e.g., several μs), pulses that occur within 20-μs after a higher amplitude pulse are handled as reflections and they are removed.

Consequently, the following six feature vectors are obtained: two peak vectors ($\mathbf{p}_A$ and $\mathbf{p}_B$), two TOA vectors ($\mathbf{t}_A$ and $\mathbf{t}_B$), and two PD polarity vectors ($\mathbf{d}_A$ and $\mathbf{d}_B$), as drawn in Fig .11.

B. Suppression of INIs using a pulse TOA-polarity (PTP) criterion

The location of a PD in the target CC line section is inherently different from that of INIs, which always come from the outside of this line section, e.g., another PD or switch noises from other power equipment connected to this line section. Thus, calculations based on a time-correlation analysis of the TOAs of pulses in the two signals ($\mathbf{x}'_A$ and $\mathbf{x}'_B$) are used to separate PDs and INIs. The TOA difference between the two detected pulses from the same PD on this line section must be smaller than the total propagation time T from Side A to Side B, while that of INIs outside the line section is always equal to T. In addition, since time-correlation analysis alone is insufficient to separate the PDs occurring around terminals (i.e., Side A or Side B) from the INIs, the polarity of pulses in the double-sided signals is used. It is important to point out that since the developed PD detector measures the travelling wave current component of the PD pulse in CC lines, the polarity of a measured pulse depends on its propagation direction. Pulses from the same PD on a target CC line (i.e. pulses generated within the line section at hand) have inverse polarities, due to their different directions of propagation. In contrast, the INIs from other CC lines or apparatus out of the range of the target CC line have the same polarities, reaching the points A and B in different time instants but exhibiting the same shape of the pulse. Thus, based on the joint application of the time-correlation and pulse polarity analysis, the following PTP criterion is defined:

$$\begin{cases} |t_{A,i} - t_{B,j}| \le T,\ t_{A,i} \in \mathbf{t}_A,\ t_{B,j} \in \mathbf{t}_B \\ d_{A,i} \cdot d_{B,j} < 0\ ,\ d_{A,i} \in \mathbf{d}_A,\ d_{B,j} \in \mathbf{d}_B \end{cases} \tag{8}$$

The pulses in $\mathbf{x}'_A$ and $\mathbf{x}'_B$ whose TOAs and polarities satisfy Equation (8) are retained, and the remainders are discarded. This process gave the results depicted in Fig. 12, wherein it can be seen that most of INIs, the amplitudes of which were slightly larger than those of the PDs, were removed. Consequently, four new feature vectors are obtained: two peak vectors ($\mathbf{p}'_A$ and $\mathbf{p}'_B$) and two TOA vectors ($\mathbf{t}'_A$ and $\mathbf{t}'_B$). The criterion is expected to effectively work due to the fact that most of INIs acquired at double sides almost rarely meet it.

C. Estimation of PD locations based on location mapping and least-squares approach

Using $\mathbf{t}'_A$ and $\mathbf{t}'_B$, a location vector $\mathbf{L}_{PD}$ that passes from the smallest to the largest value can be calculated using Equation (5). Then, $\mathbf{p}_A$ and $\mathbf{p}_B$ can be used to obtain a real PD peak vector, $\mathbf{p}_{PD}$, from the following equation:

$$p_{PD}(i) = p_A(m) \cdot e^{\alpha_{PD} \cdot L_{PD}(i)} + p_B(n) \cdot e^{\alpha_{PD} \cdot (L_{AB} - L_{PD}(i))} \tag{9}$$

where $p_A(m)$ and $p_B(n)$ are the PD peaks of the pulses from the same PD, and α_{PD} is the attenuation coefficient of the PD signal propagating on the CC line and can be estimated via an approximation formula in [23].

PD location maps are drawn using $L_{PD}(i)$ and $p_{PD}(i)$ as the horizontal coordinate and the vertical coordinate, respectively, as shown in Fig. 13. If there is a PD defect on the target CC line, its statistical concentration characteristics are clearly revealed by these maps. A mean deviation quantity, H, which is used to quantize the concentration characteristics, is defined as follows:

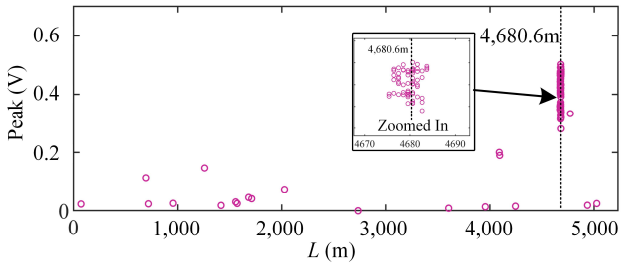

Fig. 13. PD location maps generated by the remained pulses from Fig. 12 and other five measurements on the 5232-m CC line with a PD defect (on a grimy insulator 4691 m along the line).

$$H = \frac{\sum_{i=1}^{N}(L_{PD}(i) - \bar{L}_{PD})}{N \cdot L_{AB}} \quad (L_{PD}(i) \in \mathbf{L}_{PD}) \tag{10}$$

where $\bar{L}_{PD}$ is the mean value of $\mathbf{L}_{PD}$. To automatically identify if a target CC line has a PD defect, a binary variable (B) is used, and is defined as follows

$$B = \begin{cases} 0 & H > k, \text{ there is no PD defect} \\ 1 & H < k, \text{ there is a PD defect} \end{cases} \tag{11}$$

where k is a boundary between data concentration and deconcentration, which is empirically set to be 0.05 according to the data from a dozen detected PD defects. Once it is confirmed that a PD defect is present, least-squares approach is used to statistically estimate the location of the PD defect. An optimal estimate of the location of the PD defect, x_{PD}, is calculated as follows:

$$\min_{x_{PD}} \sum_{i \in \mathbf{I}} (L_{PD}(i) - x_{PD})^2 \tag{12}$$

where $\mathbf{I} = \{i \mid \bar{L}_{PD} - 0.1L_{AB} \le L_{PD}(i) \le \bar{L}_{PD} + 0.1L_{AB}\}$.

The concentration characteristics analysis and the least-squares estimation could statistically minimize the negative effect of the rest of INIs and TOA errors on PD localization.

In addition, it should be mentioned that a few CC lines may contain more than one PD source or another corona (collectively referred to as discharge). An approach to handle this situation is briefly discussed as follows. Since their locations are usually different, multiple clusters of discharge events can occur in the PD location map. The number and locations of the clusters can be determined via the probability density curve of $\mathbf{L}_{PD}$, in which significant peaks can occur in the locations of the discharge sources. Their number is determined as the number of the peaks of the probability density curve, and their locations correspond to the locations of the peaks. Then, $\mathbf{L}_{PD}$ can be cut into multiple sections, one of which should contain only one cluster (i.e., one discharge source). Finally, the locations of the discharge sources are estimated by applying the above-described algorithm to each section. With the locations of the discharge sources, the technician can further identify the exact types of the discharge sources via the conventional vision- and ultrasonic-based tools, e.g., the widely used ultrasonic camera, which are available in most distribution maintenance teams.

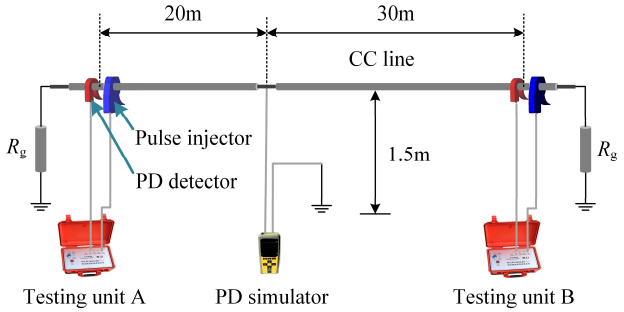

Fig. 14. Setup of the test platform.

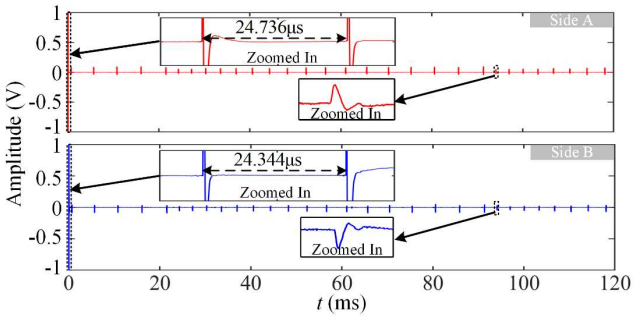

Fig. 15. Acquired waveforms on Side A and Side B of the measured CC line. The zoomed-in insets display the waveform details of the injected high amplitude pulses and simulated PD pulses.

V. Laboratory and Field Validation

A. *Laboratory Validation of the proposed PD location method and system*

To validate the performance of the proposed PD location method and system, a laboratory experiment was carried out on a 50-m single-phase 10-kV CC line, which was 14-mm in diameter and had a 2-mm layer of insulation. The test platform is depicted in Fig. 14. The CC line was positioned 1.5 m above the ground, and each end of the line was connected to a separate terminal resistor R_g (300 Ω) to simulate a load. A programmable PD simulator, which produces a series of pulses with waveforms similar to those of PDs, was used to simulate PDs, and was mounted on the CC line 20 m from Side A. The apparent charge magnitude of the pulses produced by the simulator was programmed to vary from approximately 4 to 10-nC. The signals recorded by the two testing units are shown in Fig. 15. The injected pulses locate at the start of the acquired signals. Calculations of the TOAs of the injected pulses reveal that the pulse traveled from Side A to Side B in 188 ns, which equates to a pulse propagation velocity of 265.9 m/μs.

60 PD localizations, driven by GPSM (30 localizations) and GPS (30 localizations), respectively, were calculated, and the statistical results of mapping these locations are given in Fig. 16. The results show that the maximum error and mean error of the PD localizations driven by the GPS synchronization were 15.94-m and 5.82-m, respectively, whereas those of the PD localizations driven by the GPSM were 2.87 m and 0.79 m. The primary reason why the GPS-based PD localization has larger errors is that synchronization errors of the PPS outputs of the GPS were always within a range of approximately hundreds of

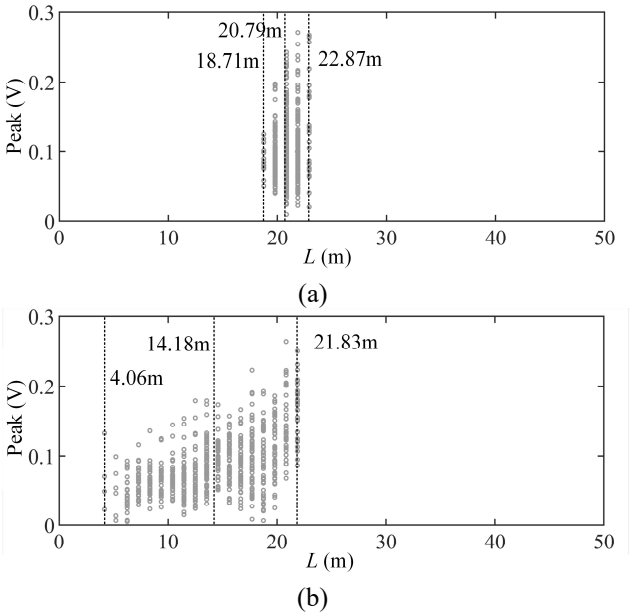

Fig. 16. PD location mappings based on the improved PD location method driven by GPSM (a) and the classical PD location method driven by GPS (b), respectively.

TABLE I
Comparison of the PD localization between GPSM and PS.

Apparent charge magnitude of the pulses produced by the PD simulator	Mean value of PD locations	
	GPSM	PS
<56 nC	20.83 m	20.82 m
⩾56 nC	20.74 m	*Error*

nanoseconds. It is expected that the errors of PD localizations driven by the GPS modules would be even larger during field testing, due to complex environmental factors and propagation velocity errors caused by the unknowing propagation parameters in CC lines.

Then, the maximum apparent charge magnitude of the outputs of the PD simulator was gradually increased from 10nC to 200nC. The localization results, driven by GPSM and pulse synchronization (PS) (which depends on a threshold triggering mode, referring to [14]), respectively, are listed in Tab. 1. As the apparent charge magnitude of the simulated pulses is greater than 56nC, the PS-based method with a 500 mV trigger threshold is failed to obtain the PD localization results. It demonstrates that the reliability of the PS-based location method is associated with the magnitudes of the injected pulses and PDs, and is expected to be lower when it is used on a long CC line (eg. 10km) due to the inevitable high-frequency propagation attenuation. In contrast, the GPSM-based location method is still reliable because it uses GPSs to trigger the signal acquisitions. In conclusion, the GPSM-based PD location method locates PDs in CC lines more accurately and reliably than conventional GPS-based and latest PS-based methods.

In addition, simulated noise disturbances (i.e., CNIs, including white noise and discrete spectrum noise) are added into the measured noiseless PD data to test the accuracy of the proposed algorithm, as shown in Fig. 17. The frequencies of

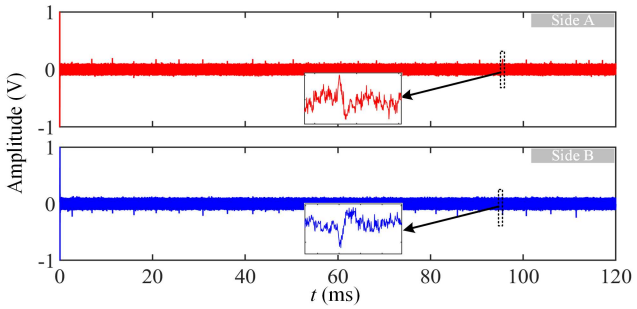

Fig. 17. Waveforms of synthetic noisy PD signals with a signal-to-noise ratio of -13.3 dB.

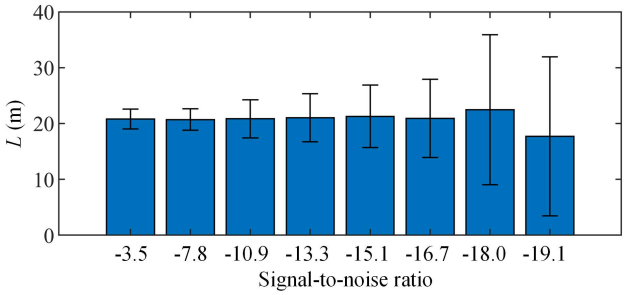

Fig. 18. Results of PD location estimations under varying signal-to-noise ratios.

two harmonics in the discrete spectrum noise are set to 1 and 6 MHz and their corresponding amplitudes are set to 0.045 and 0.03 V, respectively. White noise is a zero mean gaussian sequence with 0.03 V standard deviation. The signal-to-noise ratio of the synthetic PD signals can be tuned by proportionally scaling the amplitudes of the noises. Figure 18 collects the PD location estimate results under varying signal-to-noise ratios. It can be observed that as the signal-to-noise ratio decreases, the standard deviation of the PD locations becomes unavoidably larger. However, the procedure arising from (12) is robust and it coherently produces the correct estimate of the actual value of the PD location (i.e., 20 m). In other words, that means that although the CNIs can lead to uncertain errors on one PD location estimate, the statistical mean of multiple estimated PD locations is beneficial for very low signal-to-noise ratio scenario, demonstrating the effectiveness and robustness of the proposed algorithm.

B. Field application example

An on-site testing was conducted on a 2125-m long and approximately 12-m high 10-kV CC line in a town in Jiangsu province, China. The installed test system is shown in Fig. 19. The length of the CC line was calculated as the sum of the straight-line distances between all towers in the range of the CC line. The PD detectors and the pulse injectors were safely and conveniently installed using long insulating rods.The injected pulses, the acquired original signals, the processed signals, and the PD location results are all displayed in Fig. 20 and are discussed below.

The injected pulses recorded by the testing units are shown in Fig. 20(a) and (b); it can be seen that a pulse traveled from Side A to Side B in 7.864 μs, which equates to a pulse

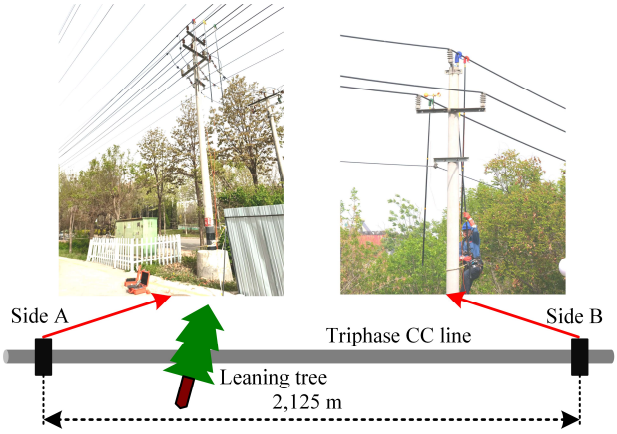

Fig. 19. Installation of the on-line PD location system on the double sides of a 2125-m CC line. The red, green, and yellow PD detectors are mounted on Phase 1, Phase 2, and Phase 3 of the line, respectively, and the blue PD injector is mounted on Phase 1 of the line.

propagation velocity of 270.2 m/μs. As shown in Fig. 20(c)-(h), the original signals were acquired by all of the PD detectors on both sides. The original signals contained representative CNIs and INIs that obscured useful PD pulses. These original signals were de-noised using the DWT, which gave the de-noised signals shown in Fig. 20(i)-(n). It can be seen that the CNIs were suppressed, such that some pulses with magnitudes less than the CNIs were revealed, as in the rear half of the waveform in Fig. 20(l). Next, the TOAs, peaks, and polarities of the pulses were extracted, as shown in Fig. 20(o) and (p). Then, the PTP criterion was applied to the all extracted pulses. It can be seen that most of INIs were removed, though their amplitudes were greater than those of the PD pulses (Fig. 20(q) and (r)). The remaining pulses had power-frequency correlation patterns that were typical of PDs. Moreover, as the peaks of the pulses in Phase 1 were higher than those of the pulses in the other two phases, and the pulse polarities of Phase 1 were opposite to those of the other two phases, the PDs were easily identified as being in Phase 1. Finally, the location map was constructed, as shown in Fig. 20(s), which clearly shows that the PD source was located 282.7 m from Side A. It is important to point out that although a few spurious location estimates occur in the PD location map, which is caused by the residual INIs, the final location estimate result is still accurate because it is obtained via the statistical concentration characteristics of all location estimates.

To further identify defect types, a commercial ultrasonic PD-detection camera (NL100 Camera, NL) was used to identify the exact position of the defect from the location imaging result and a picture of part of the tree leaning on the line are shown in Fig. 21. The location error was calculated to be 6.9 m (0.32% of the length of the CC line). Accordingly, the staff trimmed the tree and subsequently conducted a second PD test on the CC line. No PD signals were found, thereby confirming that the tree had been the cause of the PDs. The entire testing process—including the installation, signal collection, and data analysis—was completed within 15 min, which is a significantly shorter period of time than that required for conventional ultrasonic inspections (~60 min, which could be supposed to be longer for CC lines in forest or areas without sidewalks).

VI. Conclusion

This paper proposes an innovative PD location technique for 10-kV overhead CC lines, achieved by an improved double-sided TW method based on a hybrid time-synchronization technique, namely GPSM. It integrates GPS's stability and PSM's accuracy to enable accurate and reliable PD localization, which is verified with laboratory experiments.

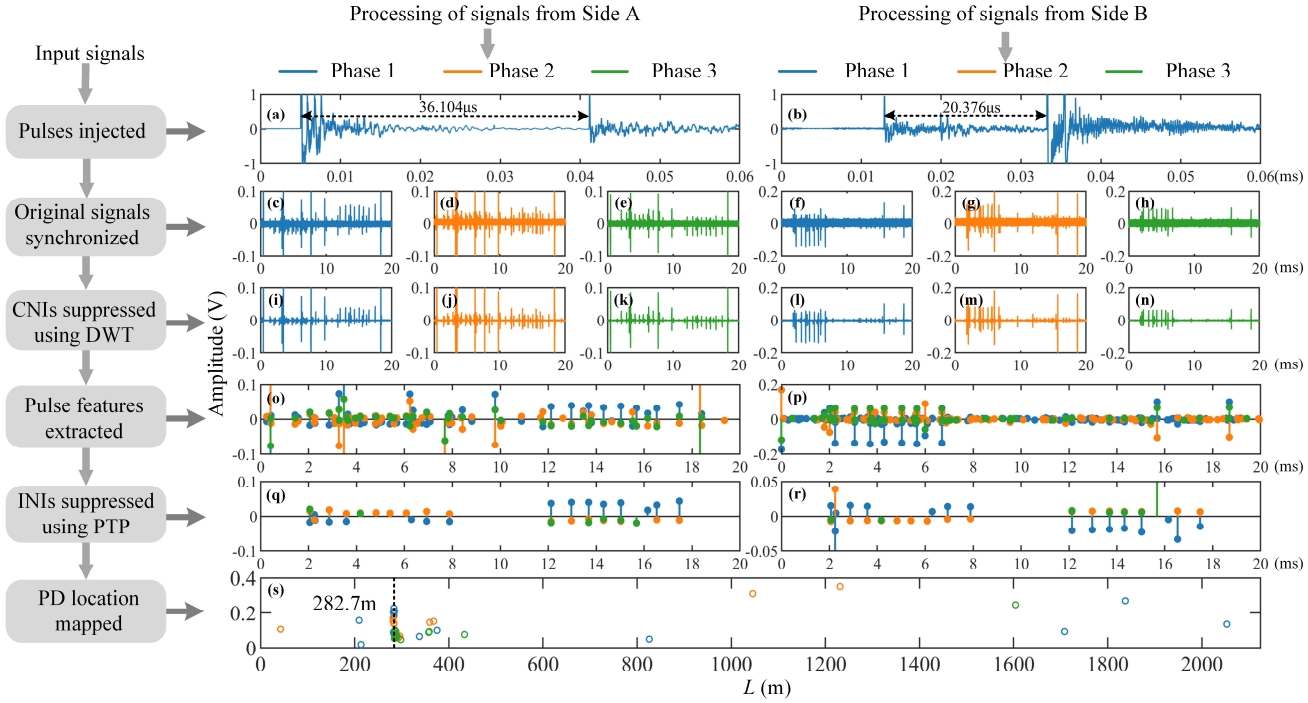

Fig. 20. Signal processing and location result of the PD measurement on the 2125-m three-phase overhead CC line.

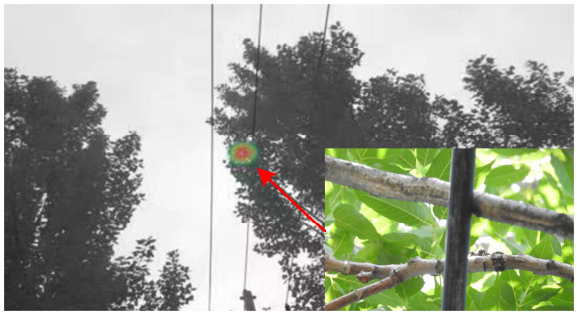

Fig. 21. Ultrasonic imaging of the detected PD defect, captured using a commercial ultrasonic camera (NL100 Camera, NL). The inset shows a picture of the tree leaning on the CC line.

A practical on-line PD location system and an enhanced PD location algorithm are developed. The proposed system consists of two portable and non-invasive testing units and a cloud server. Modified HFCTs, inductive pulse injectors, and optical fiber transmissions are used in each testing unit, guaranteeing both safety and modularity. The location algorithm incorporates the signal processing of received signals via DWT to suppress CNIs and a PTP criterion to suppress INIs. A least-squares approach applied to the location maps is also adopted for accurate PD localization. The effectiveness of the wrapped up system was verified through on-site testing on a 2125-m 10-kV CC line. The total location error was less than 0.5%, allowing electric utilities to clearly determine where condition-based maintenance is required.

It is important to remark that the proposed on-line PD location technique can be used as to provide an additional important support to the conventional vision- and ultrasonic-based inspection methods, allowing to further improve the efficiency of on-site PD measurement of CC lines. In addition, it turns out to be particularly well suited for the CC lines in spacious forest, farming, and stockbreeding areas, where it is quite difficult for technician to patrol the widely distributed CC lines via the vision- and ultrasonic-based methods, due to lack of sidewalks.

ACKNOWLEDGEMENT

This work was supported in part by Taizhou Power Supply Branch of State Grid Jiangsu Electric Power Co., LTD. Thanks to Jianguang Yao, Tailong Sun, and Zhongjun Jiang for assistance with the field experiments.

REFERENCES

[1] G. C. Montanari, R. Hebner, P. Seri and R. Ghosh, “Self-Assessment of Health Conditions of Electrical Assets and Grid Components: A Contribution to Smart Grids,” in *IEEE Transactions on Smart Grid*, vol. 12, no. 2, pp. 1206-1214, March 2021.

[2] G. C. Montanari and A. Cavallini, “Partial discharge diagnostics: from apparatus monitoring to smart grid assessment,” in *IEEE Electrical Insulation Magazine*, vol. 29, no. 3, pp. 8-17, May-June 2013.

[3] R. Bartnikas, "Partial discharges. Their mechanism, detection and measurement," in *IEEE Transactions on Dielectrics and Electrical Insulation*, vol. 9, no. 5, pp. 763-808, Oct. 2002.

[4] G. M. Hashmi, M. Lehtonen and M. Nordman, “Modeling and experimental verification of on-line PD detection in MV covered-conductor overhead networks,” in *IEEE Transactions on Dielectrics and Electrical Insulation*, vol. 17, no. 1, pp. 167-180, Feb. 2010.

[5] B. Lee, S.Choi, and Y. Jung, “Field experience of diagnosis techniques for detecting damaged Insulators of overhead distribution line,” in *Proc. CIRED - 22th Int. Conf. Exhib. Elect.Distribution - part 2*, 2013, pp. 1471.

[6] S. Suwanasri *et al*., “Partial Discharge Investigation and Failure Analysis on Distribution Network Using Acoustic Camera,” *2021 9th International Electrical Engineering Congress (iEECON)*, 2021, pp.

[7] S. C. Fernando, W. S. T. Rowe and K. L. Wong, “Long Wire Antenna-Like Behavior of Uninsulated Overhead Distribution Cables,” in *IEEE Transactions on Power Delivery*, vol. 27, no. 3, pp. 1116-1123, Jul. 2012.

[8] M. Krátký, S. Mišák, P. Gajdoš, P. Lukáš, R. Bača, and P. Chovanec, “A Novel Method for Detection of Covered Conductor Faults in Medium Voltage Overhead Line Systems,” in *IEEE Transactions on Industrial Electronics*, vol. 65, no. 1, pp. 543-552, Jan. 2018.

[9] J. Fulneček and S. Mišák, “A Simple Method for Tree Fall Detection on Medium Voltage Overhead Lines With Covered Conductors,” in *IEEE Transactions on Power Delivery*, vol. 36, no. 3, pp. 1411-1417, Jun. 2021.

[10] S. Misák, J. Fulnecek, T. Vantuch, T. Buriánek and T. Jezowicz, “A complex classification approach of partial discharges from covered conductors in real environment,” in *IEEE Transactions on Dielectrics and Electrical Insulation*, vol. 24, no. 2, pp. 1097-1104, April 2017.

[11] L. Lu, K. Zhou, Z. Guangya, X. Yang and B. Chen, "Partial discharge location algorithm based on total least-squares with Matern kernel in cable systems," in *IEEE Transactions on Industrial Informatics*, doi: 10.1109/TII.2022.3153835.

[12] F. P. Mohamed, W. H. Siew, J. J. Soraghan, S. M. Strachan and J. McWilliam, “Partial discharge location in power cables using a double ended method based on time triggering with GPS,” in *IEEE Transactions on Dielectrics and Electrical Insulation*, vol. 20, no. 6, pp. 2212-2221, December 2013.

[13] H. Li, X. Cui, H. Wang, Y. Yan, Y. Lu and K. Zhao, “A Novel Partial Discharge Locating System for 10-kV Covered Conductor Lines in Distribution Network,” *2020 10th International Conference on Power and Energy Systems (ICPES)*, 2020, pp. 379-383.

[14] W. He, H. Sun, H. Li, D. Liang, Z. Sun and B. Liu, “A Novel Time Alignment Technique for Online PD Location in Covered Conductors,” in *IEEE Transactions on Power Delivery*, vol. 31, no. 6, pp. 2559-2561, Dec. 2016.

[15] W. He, H. Li, D Liang *et al*, “Implementation of a Novel Double-side Technique for Partial Discharge Detection and Location in Covered Conductor Overhead Distribution Networks,” in *Meas. Sci. Technol*. vol. 26, no. 12, pp. 125009, Dec. 2016.

[16] P. C. J. M. van der Wielen, P. A. A. F. Wouters, J. Veen and D. M. van Aartrijk, "Synchronization of on-line PD detection and localization setups using pulse injection," Proceedings of the 7th International Conference on Properties and Applications of Dielectric Materials (Cat. No.03CH37417), 2003.

[17] M. Isa, N. I. Elkalashy, M. Lehtonen, G. M. Hashmi and M. S. Elmusrati, “Multi-end correlation-based PD location technique for medium voltage covered-conductor lines,” in *IEEE Transactions on Dielectrics and Electrical Insulation*, vol. 19, no. 3, pp. 936-946, Jun. 2012.

[18] Soltani, Amir Abbas, and Seyyed Mohammad Shahrtash. “Decision tree –based method for optimum decomposition level determination in wavelet transform for noise reduction of partial discharge signals,” in *IET Science, Measurement & Technology*, vol. 14, no. 1, pp. 9-16, 2020.

[19] X. Ma, C. Zhou and I. J. Kemp, "Automated wavelet selection and thresholding for PD detection," in *IEEE Electrical Insulation Magazine*, vol. 18, no. 2, pp. 37-45, March-April 2002.

[20] “IEEE Guide for Maintenance Methods on Energized Power Lines,” in *IEEE Std 516-1995*, pp.1-72, 30 Jun. 1995.

[21] L. She, Z. Xu, S. Zhang, and Y. Song, “De-noisng of ECG based on EMD improved-thresholding and mathematical morphology operation,” in *Proc. 3rd Int. Conf. Biomed. Eng. Informat.*, Yantai, China, Oct. 2010, pp. 838–842.

[22] P. Wagenaars, P. A. A. F. Wouters, P. C. J. M. van der Wielen and E. F. Steennis, “Accurate estimation of the time-of-arrival of partial discharge pulses in cable systems in service,” in *IEEE Transactions on Dielectrics and Electrical Insulation*, vol. 15, no. 4, pp. 1190-1199, Aug. 2008.

[23] G. M. Hashmi, M. Lehtonen and M. Nordman, “Calibration of on-line partial discharge measuring system using Rogowski coil in covered-conductor overhead distribution networks,” in *IET Science, Measurement & Technology*, vol. 5, no. 1, pp. 5-13, January 2011.

Yuan Yan was born in Sichuan, China, in 1996. He received the B.S. degree in electrical engineering from Xi'an Jiaotong University, Xi'an, China, in 2018.

He is currently working toward the Ph.D. degree in electrical engineering with Xi'an Jiaotong University, Xi'an, China, and also with Department of Electronics and Telecommunications, Politecnico di Torino, Turin, Italy. His research mainly focuses on the insulation condition monitoring of electrical equipment, modeling of electromagnetic, and signal processing.

Yinsong Zhao was born in Jilin, China, in 1998. He received the B.S. degree in electrical engineering from Xi'an Jiaotong University, Xi'an, China, in 2021.

He is currently working toward the M.S. degree in electrical engineering with Xi'an Jiaotong University, Xi'an, China. His research mainly focuses on the insulation condition monitoring of electrical equipment.

Weisheng He was born in Chongqing, China. He received the B.S. and Ph.D. degrees in electrical engineering from Xi'an Jiaotong University, Xi'an, China, in 2013 and 2018, respectively.

From 2018 to 2021, he was a postdoctor and executive engineer in State Grid Chongqing Electric Power Research Institute, Chongqing, China. Currently, he is a lecturer with the Chongqing Key Laboratory of Complex Systems and Bionic Control, Chongqing University of Posts and Telecommunications, Chongqing, China. His major research interests include insulation condition monitoring of the electrical equipments, modeling and numerical analysis of electromagnetic devices.

Igor Simone Stievano (M'98–SM'08) received the master's degree in electronic engineering and the Ph.D. degree in electronics and communication engineering from the Politecnico di Torino, Turin, Italy, in 1996 and 2001, respectively. He is currently a Professor of Electrical Engineering with the Department of Electronics and Telecommunications, Politecnico di Torino. In the period 2017-2021, he was the Vice Rector of Academic and Scientific Activities of the joint campus of the Politecnico di Torino in Uzbekistan, Turin Polytechnic University in Tashkent (TTPU). Also, he was the Program Co-Chair of the 20th and 21st IEEE Workshops on Signal and Power Integrity (SPI2016 and SPI2017). He has authored or coauthored more than 130 papers published in international journals and conference proceedings. His current research interests include electromagnetic compatibility and signal integrity, with emphasis on modeling and simulation of digital circuits, transmission lines, PLC channels, switching converters, development of stochastic methods for the statistical simulation of circuits and systems, and the compact modeling of electrical and gas networks via a complex network paradigm and simplified graph-based approaches.

Hongjie Li was born in Henan, China, in 1966. He received the B.S., M.S., and the Ph.D. degrees from Xi'an Jiaotong University, Xi'an, China, in 1989, 1992, and 1998, respectively.

In 1997, he was a Visiting Scholar at Osaka University, Osaka, Japan. From 1999 to 2001, he was a Research Fellow on insulation condition monitoring at Nanyang Technological University, Singapore. And then he was employed in Singapore power grid company, Ltd. from 2001 to 2007. Currently, He is a professor with the High Voltage Division, School of Electrical Engineering, Xi' an Jiaotong University. His major research interests include insulation condition monitoring of the electrical equipment, modeling and numerical analysis of electromagnetic.